Quantum-noise randomized data-encryption for WDM fiber-optic networks

Eric Corndorf,* Chuang Liang, Gregory S. Kanter, Prem Kumar, and Horace P. Yuen

Center for Photonic Communication and Computing,
Department of Electrical and Computer Engineering,
Northwestern University
2145 Sheridan Road, Evanston, IL 60208
(Dated: February 1, 2008)

We demonstrate high-rate randomized data-encryption through optical fibers using the inherent quantum-measurement noise of coherent states of light. Specifically, we demonstrate 650Mbps data encryption through a 10Gbps data-bearing, in-line amplified 200km-long line. In our protocol, legitimate users (who share a short secret-key) communicate using an M-ry signal set while an attacker (who does not share the secret key) is forced to contend with the fundamental and irreducible quantum-measurement noise of coherent states. Implementations of our protocol using both polarization-encoded signal sets as well as polarization-insensitive phase-keyed signal sets are experimentally and theoretically evaluated. Different from the performance criteria for the cryptographic objective of key generation (quantum key-generation), one possible set of performance criteria for the cryptographic objective of data encryption is established and carefully considered.

I. INTRODUCTION

For more than twenty years, physicists and engineers have investigated quantum-mechanical phenomena as mechanisms to satisfy certain cryptographic objectives. Such objectives include user authentication, bit commitment, key generation, and recently, data encryption. To date, the cryptographic objective most considered in the literature has been key generation. In key generation, two users, who initially share a small amount of secret information, remotely agree on a sequence of bits that is both larger than their original shared information and is known only to them. The newly generated bits (keys) are then used to publicly communicate secret messages over classical channels by driving data encrypters like the information-theoretically perfect one-time pad [1] or more efficient (but less secure) encrypters, such as the Advanced Encryption Standard, where security is described in terms of complexity assumptions [2, 3].

Several approaches to key generation using quantum effects have been proposed and demonstrated. The most famous of these protocols, the BB84 protocol [4] and the Ekert protocol [5] have enjoyed considerable theoretical consideration as well as experimental implementation [6, 7, 8]. A major technical limitation of the BB84 (Ekert) protocol is that the achievable key-generation rate (more importantly, the rate-distance product) is relatively low due to the protocol's requirement for single-photon (entangled-photon) quantum states. This requirement is a burden not only in the generation of such states, but also in that such states are acutely susceptible to loss, are not optically amplifiable (in general), and are

difficult to detect at high rates. Furthermore, because the received light must be detected at the single-photon level, integration of the protocol implementations into today's wavelength-division-multiplexed (WDM) fiber-optic infrastructure is problematic because cross-channel isolation is typically no better than 30dB.

Recently, we have demonstrated a new quantum cryptographic scheme, based on Yuen's KCQ approach [9], in which the inherent quantum noise of coherent states of light is used to perform the cryptographic service of data encryption [10, 11]. Unlike single-photon states, coherent states (of moderate average-energy level) are easily generated, easily detected, and are optically amplifiable, networkable, and loss tolerant. Note that key generation and data encryption are two *different* cryptographic objectives with *different* sets of criteria by which to judge performance—a direct comparison between the two is not appropriate.

In our scheme, legitimate users extend a short, shared secret-key by using a publicity known deterministic function. The transmitter uses the extended key to select a signal set for each transmitted bit such that the legitimate receiver, using the same extended key, is able to execute a simple binary-decision measurement on each bit. An eavesdropper, on the other hand, who does not possess the secret key, is subject to an irreducible quantum uncertainty in each measurement, even with the use of ideal detectors. This uncertainty results in randomization of the eavesdropper's observations, thereby realizing a true randomized cipher [12] which effectively limits the eavesdropper's ability to decipher the transmitted message. This randomization is "free" in that it does not require any additional action on the part of the transmitter in contrast to other randomized ciphers [13, 14], where active randomization of the signal-set is required by the transmitter. Our scheme, running at data-encryption rates up to 650Mbps, uses off-the-shelf components and

is compatible with today's optical telecommunications infrastructure. This paper is organized as follows: in section II we outline our quantum-noise protected data-encryption protocol (call the $\alpha\eta$ protocol), in section III we address issues of security and performance, and in section IV we summarize our experimental results.

II. DATA ENCRYPTION PROTOCOL

We have implemented two versions of our quantum-noise protected data-encryption protocol using different signal sets—one using polarization states [11] (polarization-mode scheme) and the other using phase states [15, 16] (time-mode scheme). In both implementations, the fundamental and irreducible measurement uncertainty of coherent states is the key element giving security. In the polarization-mode scheme, the two-mode coherent states employed are

$$|\Psi_m^{(a)}\rangle = |\alpha\rangle_x \otimes |\alpha\, e^{i\theta_m}\rangle_y, \tag{1}$$

$$|\Psi_m^{(b)}\rangle = |\alpha\rangle_x \otimes |\alpha\, e^{i(\theta_m+\pi)}\rangle_y, \tag{2}$$

where $|\alpha\rangle$ is a coherent state, $\theta_m = \pi m/M$, $m \in \{0, 1, 2, ..., (M-1)\}$, M is odd, and the subscripts x and y indicate the two orthogonal polarization mode-functions. Viewed on the Poincaré sphere, these $2M$ polarization states form M bases that uniformly span a great circle as shown in Fig. 1(top). In the time-mode scheme, the single-mode coherent states employed are

$$|\Psi_m^{(a)}\rangle = |\alpha e^{i\theta_m}\rangle, \tag{3}$$

$$|\Psi_m^{(b)}\rangle = |\alpha e^{i(\theta_m+\pi)}\rangle, \tag{4}$$

where again $\theta_m = \pi m/M$, $m \in \{0, 1, 2, ..., (M-1)\}$, and M is odd. These $2M$ states form M antipodal-phase pairs (bases) that uniformly span the phase circle, as shown in Fig. 1(bottom).

In both schemes, the transmitter (Alice) extends an s-bit secret key, $\mathbf{K}$, to a $(2^s - 1)$-bit pseudo-random extended-key, $\mathbf{K}'$, using a publicly known s-bit linear feedback shift-register [2] (LSFR) of maximal length. The extended-key is grouped into continuous disjointed r-bit blocks and then passed through an invertible r-bit–to–r-bit deterministic mapping function, referred to as a "mapper," resulting in running-keys, $\mathbf{R}$, where $r = \mathrm{Int}[\log_2 M]$ and $s \gg r$. The mapper, which is publicly known, helps to distribute an attacker's measurement uncertainty throughout each running-key. Without the use of a mapper, an attacker's measurement uncertainty would, the majority of the time, obscure just a the least-significant bits of each r-bit running-key thereby leaving most of the r bits clearly identifiable. Also, note that an LFSR is just one of many of functions that the users can use to extend $\mathbf{K}$ into $\mathbf{K}'$. The reason LFSRs are used in these experiments is because they are mathematically simple to describe which could be useful when quantifying the precise level of security provided by $\alpha\eta$.
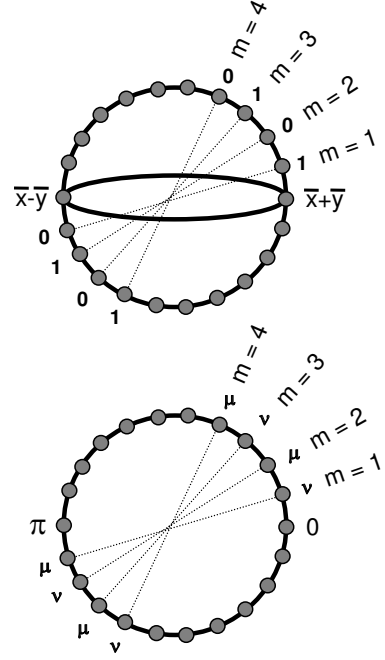

FIG. 1: Top: M pairs of orthogonal polarization states uniformly span a great circle of the Poincaré sphere; Bottom: M pairs of antipodal phase states uniformly span a phase circle.

Depending on the data bit and an instantiation of the running-key R, one of the states in Eqs. (1) [(3)] or (2)[(4)] is transmitted where m is the decimal representation of R. Specifically, for the polarization-mode scheme, if m is even then $(0,1) \rightarrow (|\Psi_m^{(a)}\rangle, |\Psi_m^{(b)}\rangle)$ and if m is odd then $(0,1) \rightarrow (|\Psi_m^{(b)}\rangle, |\Psi_m^{(a)}\rangle)$. This results in the logical bit mapping of the polarization states on the Poincaré sphere to be interleaved $0, 1, 0, 1, ...$, as shown in Fig. 1(top). The time-mode scheme is similarly organized but slightly more complicated in that the data bits are defined differentially (differential-phase-shift keying, DPSK). Specifically, if m is even, then the DPSK mapping is $(0, \pi) \rightarrow (|\Psi_m^{(a)}\rangle, |\Psi_m^{(b)}\rangle)$, and $(0, \pi) \rightarrow (|\Psi_m^{(b)}\rangle, |\Psi_m^{(a)}\rangle)$ for m odd. If we relabel the states corresponding to DPSK phases of "0" and "π" as μ and ν, respectively, then logical zero is mapped to $|\Psi_m^{(\mu)}\rangle$ ($|\Psi_m^{(\nu)}\rangle$) if the previously transmitted state was from the set $\{|\Psi_m^{(\mu)}\rangle\}$ ($\{|\Psi_m^{(\nu)}\rangle\}$) and logical one is mapped to $|\Psi_m^{(\mu)}\rangle$ ($|\Psi_m^{(\nu)}\rangle$) if the previously transmitted state was from the set $\{|\Psi_m^{(\nu)}\rangle\}$ ($\{|\Psi_m^{(\mu)}\rangle\}$). This results in the mapping of the symbols on the phase circle to be interleaved $\mu, \nu, \mu, \nu, ...$, as shown in Fig. 1(bottom).

At the receiving end, the intended receiver (Bob) uses the same s-bit secret key and LFSR/mapper to apply unitary transformations to his received quantum states according to the running-keys. These transformations correspond to polarization-state rotations for the polarization-mode scheme, and phase shifts for the time-mode scheme—in either case the transmitted M-ry signal

set is reduced to a binary signal-set. The resulting states under measurement, depending on the logical bit, are

$$|\Psi^{(a)}\rangle' = |\eta\alpha\rangle_x \otimes |\eta\alpha\rangle_y, \quad (5)$$

$$|\Psi^{(b)}\rangle' = |\eta\alpha\rangle_x \otimes |-\eta\alpha\rangle_y, \quad (6)$$

for the polarization-mode scheme and

$$|\Psi^{(a)}\rangle' = |\eta\alpha\rangle, \quad (7)$$

$$|\Psi^{(b)}\rangle' = |-\eta\alpha\rangle, \quad (8)$$

for the time mode scheme, where η is the channel transmissivity. For both schemes the states are then demodulated and differentially detected. Specifically, a fixed $\pi/4$ polarization rotation on the states in the polarization-mode scheme results in the detected states

$$|\widetilde{\Psi}^{(a)}\rangle = |\sqrt{2}\eta\alpha\rangle_x \otimes |0\rangle_y, \quad (9)$$

$$|\widetilde{\Psi}^{(b)}\rangle = |0\rangle_x \otimes |\sqrt{2}\eta\alpha\rangle_y, \quad (10)$$

whereas temporally-asymmetric interferometry in the time-mode implementation results in the detected states

$$|\widetilde{\Psi}^{(a)}\rangle = |\eta\alpha\rangle_1 \otimes |0\rangle_2, \quad (11)$$

$$|\widetilde{\Psi}^{(b)}\rangle = |0\rangle_1 \otimes |\eta\alpha\rangle_2. \quad (12)$$

An important feature to note is that Bob does not require high precision in applying decryption transformations to a transmitted bit. While the application of a slightly incorrect polarization/phase transformation results in a larger probability of error for the bit, it does not categorically render a bit to be in error. For small perturbations to the polarization/phase rotation, the majority of the signal energy stays in one of the two detection modes. The same applies to Bob's detector noise; while an ideal detector allows for optimized performance, a noisy detector does not limit Bob's decryption ability beyond an increased probability of bit error.

A high-level block diagram of the $\alpha\eta$ protocol is provided in Fig. 2. Note that some elements of our protocol that help to protect the secret key against attack have been intentionally omitted from this description for the purpose of clarity. These omitted elements are mentioned in the following section and are further described in Ref. [9].

III. SECURITY

As stated in the introduction, key generation and data encryption are different cryptographic objectives and, therefore, have different sets of criteria by which to evaluate performance. The delineation between key generation and data encryption is somewhat confused by terminology. Because keys procured by a key-generation protocol are usually assumed to drive deterministic encrypters, the terms "quantum key-generation"

and "quantum data-encryption" are sometimes used interchangeably. This easily leads to confusion in that (a) there are potential uses for the generated keys beyond data encryption, and (b) there are methods of realizing quantum-based data-encryption without key generation.

In quantum key-generation, a necessary (but not sufficient) condition that must be satisfied is

$$H(\mathbf{X}|\mathbf{Y^E}, \mathbf{K}) - H(\mathbf{X}|\mathbf{Y^B}, \mathbf{K}) - H(\mathbf{K}) > 0, \quad (13)$$

where $\mathbf{X}$ is a classical n-bit random vector describing the transmitted bits, $\mathbf{Y^E}$ and $\mathbf{Y^B}$ are n-bit vectors describing the observations of an attacker (Eve) and Bob, respectively; $\mathbf{K}$ is an s-bit, previously shared secret between Alice and Bob that might become public on completion of the protocol, and $H(\cdot)$ is the Shannon entropy function. Note that while often omitted in descriptions of the BB84 and Ekert protocols, both schemes require a secret key $\mathbf{K}$ for the purpose of message authentication. Also note that the $H(\mathbf{K})$ term in Eq. (13) may be omitted if both a) information about $\mathbf{K}$ is never publicly announced, and b) $\mathbf{K}$ remains secret even when under a general attack (as in some of Yuen's KCQ key-generation protocols).

The mathematical definition of $H(\mathbf{X}|\mathbf{Y})$, to be read as "the uncertainty of $\mathbf{X}$ given $\mathbf{Y}$," is given by

$$H(\mathbf{X}|\mathbf{Y}) \equiv -\sum_{\mathbf{x},\mathbf{y}} p(\mathbf{X} = \mathbf{x}, \mathbf{Y} = \mathbf{y})$$
$$\times \log p(\mathbf{X} = \mathbf{x}|\mathbf{Y} = \mathbf{y}), \quad (14)$$

which, with application of Bayes' theorem and the Law of Total Probability, becomes

$$H(\mathbf{X}|\mathbf{Y}) = -\sum_{\mathbf{x},\mathbf{y}} p(\mathbf{X} = \mathbf{x})p(\mathbf{Y} = \mathbf{y}|\mathbf{X} = \mathbf{x})$$
$$\times \log \left[\frac{p(\mathbf{X} = \mathbf{x})p(\mathbf{Y} = \mathbf{y}|\mathbf{X} = \mathbf{x})}{\sum_{\mathbf{x}'} p(\mathbf{X} = \mathbf{x}')p(\mathbf{Y} = \mathbf{y}|\mathbf{X} = \mathbf{x}')} \right]. \quad (15)$$

The conditional probability distribution $p(\mathbf{Y}|\mathbf{X})$ is completely and uniquely specified by the probability distribution of the secret key $p(\mathbf{K})$, the probability distribution of the plaintext message $p(\mathbf{X})$, and the encryption function that takes $\mathbf{X}$ to $\mathbf{Y} = E_{\mathbf{K}}(\mathbf{X})$. While $E_{\mathbf{K}}(\mathbf{X})$ is usually assumed known to the attacker via the *Kerckhoff assumption*, it is important to emphasize that the calculation of $H(\mathbf{X}|\mathbf{Y})$ also depends on the probability distributions $p(\mathbf{K})$ and $p(\mathbf{X})$ according to Eve. This means that Eve's conditional entropy $H(\mathbf{X}|\mathbf{Y})$ may change if Eve's probability distribution $p(\mathbf{X})$ changes due to the acquisition of some side-information (such as the language of the plaintext message).

For the cryptographic objective of data encryption, be it classical or quantum-noise–protected, some relevant information-theoretic quantities are:

$$\text{i)} \quad H(\mathbf{X}|\mathbf{Y^B}, \mathbf{K}), \quad (16)$$

$$\text{ii)} \quad H(\mathbf{X}|\mathbf{Y^E}), \quad (17)$$

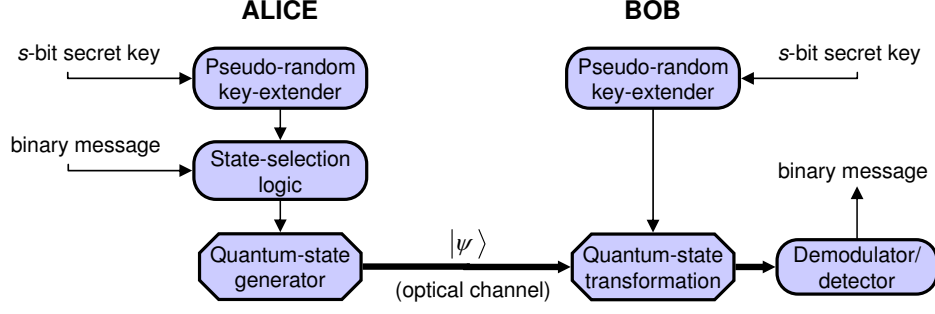$$\text{iii)} \quad H(\mathbf{K}|\mathbf{Y^E}), \quad (18)$$

FIG. 2: Summary of the quantum-noise protected data encryption protocol. In our experiments, the "pseudo-random key-extender" is implemented by a maximal-length LFSR and "r-bit–to–r-bit mapping function".

where $\mathbf{X}$ is the n-bit transmitted message (plaintext), $\mathbf{Y^B}$ and $\mathbf{Y^E}$ are Bob's and Eve's n-bit observations of the encrypted plaintext (ciphertext), and $\mathbf{K}$ is the s-bit secret key shared by the legitimate users. In words, these quantities describe i) the error rate for the legitimate users, ii) the secrecy of the data bits when under attack, and iii) the secrecy of the secret key when under attack.

When launched on either the data bits or the secret key, cryptographic attacks are normally divided into two categories, known-plaintext (KPT) attacks and ciphertext-only (CTO) attacks. CTO attacks correspond to situations where $p(\mathbf{X})$ is uniform, according to the attacker. In other words, all 2^n possible messages are transmitted with equal probability. A KPT attack corresponds to all situations where $p(\mathbf{X})$ is nonuniform including the totally degenerate deterministic case of chosen-plaintext. Some example KPT attacks include knowledge of the native language of the message or perhaps some statistical knowledge of the message content. While there are clearly varying degrees of KPT attacks, a CTO attack refers to the specific case of uniform $p(\mathbf{X})$.

According to information theory [17, 18], Eqs. (17) and (18) satisfy the following inequalities:

$$H(\mathbf{X}|\mathbf{Y^E}) \leq H(\mathbf{K}), \qquad (19)$$
$$H(\mathbf{K}|\mathbf{Y^E}) \leq H(\mathbf{K}), \qquad (20)$$

where Eq. (19) is known as the Shannon limit [19] which is valid when $H(\mathbf{X}|\mathbf{Y^E}, \mathbf{K}) = 0$ (our data-encryption protocol operates in a regime where $H(\mathbf{X}|\mathbf{Y^E}, \mathbf{K}) \cong 0$[23]). Note that in $\alpha\eta$, contrary to the case for key generation [cf. Eq. (13)], the condition $H(\mathbf{X}|\mathbf{Y^E}, \mathbf{K}) > H(\mathbf{X}|\mathbf{Y^B}, \mathbf{K})$ need *not* be satisfied. In fact the opposite is normally true where an attacker (given the secret key after measurement) has a lower bit-error rate than the legitimate receiver. This is the case when a significant amount of loss and/or additive noise exists between the two users where it is assumed that the attacker, performing an adequate quantum measurement, is located near the transmitter.

The one-time pad encrypter achieves what Shannon called "perfect security" which corresponds to $= H(\mathbf{X})$ in the inequality of Eq. (19) when $s = n$. The practical

problem with the one-time pad is that every data bit to be encrypted requires one bit of key. More "efficient," albeit less secure, encrypters operate in the regime where $s \ll n < \infty$, thereby allowing short secret-keys to encrypt long messages. A reasonable information-theoretic goal of such "imperfect but efficient" encrypters (practical encrypters) could be to show

$$H(\mathbf{X}|\mathbf{Y^B}, \mathbf{K}) \to 0, \qquad (21)$$
$$H(\mathbf{X}|\mathbf{Y^E}) = \lambda_1 \cdot H(\mathbf{K}), \qquad (22)$$
$$H(\mathbf{K}|\mathbf{Y^E}) = \lambda_2 \cdot H(\mathbf{K}), \qquad (23)$$

where $s \ll n < \infty$ and $\lambda_{1,2} \to 1$. It is extremely important to emphasize that even if $\lambda_1, \lambda_2 \to 0$, there still may exist a large complexity-based problem of finding the correct $\mathbf{x}$ even when given $\mathbf{y^E}$, $p(\mathbf{X})$, $p(\mathbf{K})$, and $E_{\mathbf{K}}(\mathbf{X})$—it is in this complexity-based limit in which all of today's commercial deterministic encrypters are considered.

According to the given information-theoretic criteria, a goal of practical data encrypters could be to a) drive $\lambda_{1,2}$ as close to 1 as possible for a reasonably large s while still keeping $s \ll n < \infty$; b) attempt to mathematically prove Eqs. (22) and (23); and c) if conditions (a) and (b) cannot be met, insure that the computational (search) complexity is high even when $\lambda_{1,2} \cdot H(\mathbf{K}) = 0$. To date, no practical data encrypter exists for which Eqs. (22) and (23) can be rigorously proven, for nontrivial λ, when under a KPT attack; no significant complexity-based security has been proven either.

Note that the appropriate information-theoretic criteria by which to quantify the security of a data encrypter may be different for different sociological situations. For example, satisfying the criteria given in Eqs. (22) and (23) ($\lambda_{1,2} = 1$) may yield security in some situations, but not in others. A different set of operationally-meaningful criteria for the cryptographic objective of data encryption, which does not rely on Shannon entropy, has been described in Ref. [9].

Towards the goal of satisfying the cryptographic objective of data encryption, according to any reasonable information-theory–based criteria, we offer a new approach to data-encryption wherein the irreducible uncertainty inherent in the quantum measurement of coherent

states of light is used to perform high-speed randomized encryption that does not sacrifice the data rate. In our protocol (section II), the logical mappings of the symbols are interleaved (Fig. 1). While the users (who share a short secret-key) are able to make simple binary decisions on the M-ry signal set, an attacker (who does not share the secret key) is left with an irreducible uncertainty in her measurements due to the quantum fluctuations inherent to coherent states of light. Specifically, with M and $|\alpha|^2$ in a particular regime, measurements of neighboring states, on either the Poincaré sphere or the phase circle, overlap and obscure one another. To an attacker, this overlap is equivalent to Alice broadcasting digital representations of the M-ry signal that are then actively randomized over the signal's closest neighbors in the signal constellation. By using coherent states with a relatively weak amplitude, a similar randomization is achieved through quantum-measurement noise which requires no active effort on the part of the transmitter, but still obscures the true identity of the state called for by the protocol. Such randomization is realized through *any* quantum measurement including direct detection, balanced homodyne/heterodyne detection, and optimal quantum-phase detection.

Given some restrictive assumptions, one can even describe the performance of a quantum-mechanically optimal attack—the best attack allowed by quantum mechanics. While the physical structure of such an optimal attack may be unknown, quantum mechanics can establish bounds on the maximum information rate of an attacker. For individual attacks on the message where classical correlations are ignored, the quantum-mechanically optimal attack—known as the optimal positive operator-valued measure—corresponds to optimally distinguishing all of the states mapped to logical one from those mapped to logical zero. Figure 3 plots the information rate of the optimal positive operator-valued measure as a function of $|\alpha|^2$ and M for the time- and polarization-mode implementations where information [17] is defined as $1 + \bar{P}_e \log_2(\bar{P}_e) + (1 - \bar{P}_e) \log_2(1 - \bar{P}_e)$ for a bit-error rate $\bar{P}_e$.

Figure 3 also plots the information rate of the described attack when performing an ideal heterodyne measurement. The performance of this measurement is included because it represents the "highest performing" receiver structure that an attacker could practically implement using today's technology. The difference between the information rates of the time- and polarization-mode implementations, for both the optimal positive operator-valued measure and ideal heterodyne attacks, is due to the fact that logical bits are defined differentially across two modes in the time-mode scheme—a bit is correctly determined if and only if two consecutive state measurements are both correct or both incorrect. It is important to remember that both the optimal positive operator-valued measure and ideal heterodyne analyses are for a very limited attack where Eve does not use her information on the correlations between the running-keys to

determine the plaintext or secret key—a real attacker would presumably use all information at her disposal.

While the inability to distinguish neighboring states plays a role in protecting the secret key against attacks, additional mechanisms are required to improve the secrecy of the secret key. By introducing deliberate state-randomization at the transmitter, perfect security against CTO attacks on the secret key $[H(\mathbf{K}|\mathbf{Y^E}) = H(\mathbf{K})$, uniform $p(\mathbf{X})]$ can be assured as well as strongly-ideal security against CTO attacks on the message $[H(\mathbf{X}|\mathbf{Y^E}) = H(\mathbf{K})$, uniform $p(\mathbf{X})]$. More information on deliberate state-randomization is available in Ref. [9]. Note that the mapper and deliberate state-randomization have not yet been implemented in our published experimental realizations.

Physical "trojan horse" attacks can also be launched on the message and the secret key by attempting to *probe* Alice's transmitter settings. In such an attack, an eavesdropper would send strong light into Alice's transmitter and measure the state of her reflected light. Attacks of this type can be passively thwarted by using an optical isolator at the output of Alice's transmitter.

Confusion over the cryptographic service that our protocol $(\alpha\eta)$ offers as well as how quantum noise is exploited in our scheme prompted a criticism [20] to Ref. [10] and some of the authors of Ref. [10] have replied [21]. In Ref. [22], it is claimed that the $\alpha\eta$ data-encryption protocol, operating in a regime where $H(\mathbf{X}|\mathbf{Y^E}, \mathbf{K}) < H(\mathbf{X}|\mathbf{Y^B}, \mathbf{K})$, already permits key generation. We disagree with that conclusion.

IV. EXPERIMENTS

Using both the polarization- and time-mode implementations, we demonstrate high-speed quantum-noise–protected data encryption. The primary objective of these experiments is to successfully demonstrate quantum data encryption through a realistic classical-data bearing WDM fiber line. A secondary objective is to show that the quantum-noise encrypted signal does not negatively impact the performance of the classical data-bearing channels. The following two subsections summarize the physical setups as well as the experimental results for both implementations.

A. Polarization-mode implementation

A description of the polarization-mode experimental setup naturally breaks into two parts: the quantum-noise–protected data-encryption transmitter/receiver pair and the WDM fiber line (which also carries classical data traffic) over which the encrypted data travels. We first describe the transmitter/receiver pair. As illustrated in Fig. 4(left), a polarization-control-paddle (PCP) is adjusted to project the light from a 1550.1nm-wavelength distributed-feedback (DFB) laser equally into
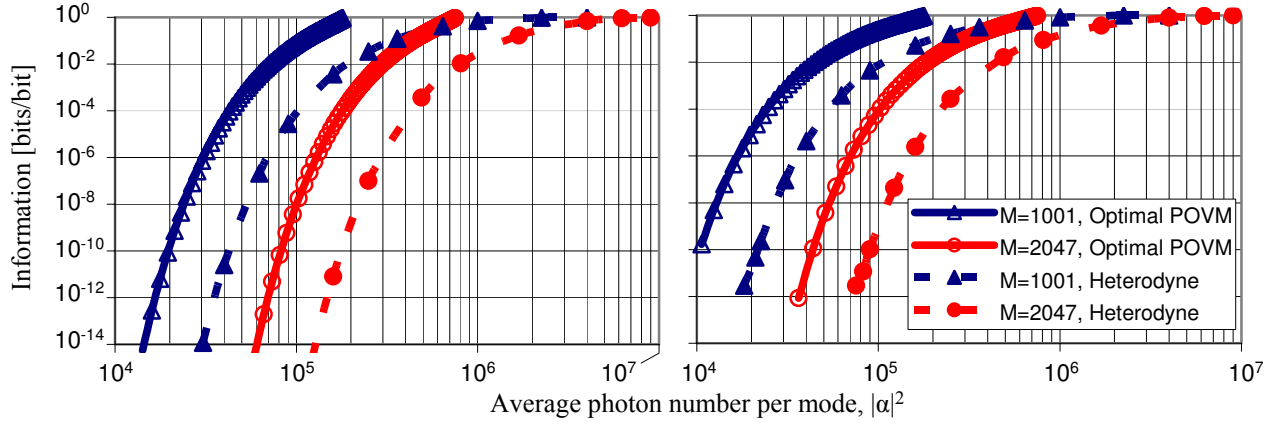
FIG. 3: Shannon information recovered through individual attacks on the message when launching either the optimal positive operator-valued measure or an ideal heterodyne measurement on the time-mode (left) and polarization-mode (right) implementations. Plotted as a function of $|\alpha|^2$, for several values of M.

the two polarization modes of Alice's 10GHz-bandwidth fiber-coupled LiNbO$_3$ phase modulator (PM). Driven by the amplified output of a 12-bit digital-to-analog (D-A) board, the modulator introduces a relative phase (0 to 2π radians) between the two polarization modes. A software LFSR, which is implemented on a personal computer (PC), yields a running-key that, when combined with the data bit, instructs the generation of one of the two states described in Eqs. (1) and (2). Due to electronic bandwidth limitations of some amplifiers, Manchester coding is applied on top of the signal set that results in a factor of two reduction of the data rate (250Mbps) relative to the line rate (500Mbps). Note that in the time-mode implementation, described in Sec. IV B, such Manchester coding is not required due to the use of wider bandwidth amplifiers.

On passing through the 100km-long WDM fiber line [shown in Fig. 4(right), *Crypto. in* and *Crypto. out*], the received light is amplified by a home-built erbium-doped–fiber amplifier (EDFA) with $\simeq$ 30dB of small-signal gain and a noise figure very close to the quantum limit (NF $\simeq$ 3dB). Before passing through Bob's PM, the received light is sent through a second PCP to cancel out the unwanted polarization rotation that occurs in the 100km-long fiber line. While these rotations fluctuate with a bandwidth on the order of kilohertz, the magnitude of the fluctuations drops quickly with frequency, allowing the use of a manual PCP to track out such unwanted polarization rotations. In future implementations Bob's measurements could be used to drive an automated feedback control on the PCP.

The relative phase shift (polarization rotation) introduced by Bob's modulator is determined by the running-key R generated through a software LFSR in Bob's PC and applied via the amplified output of a second D-A board. After this phase shift has been applied, the relative phase between the two polarization modes is 0 or π, corresponding to a 0 or 1 according to the running-key:

if R is even then $(0, \pi) \rightarrow (0, 1)$ and if R is odd then $(0, \pi) \rightarrow (1, 0)$. With use of a fiber-coupled polarization beam splitter (FPBS) oriented at $\pi/4$ radians with respect to the modulator's principal axes, the state under measurement [Eq. (9) or (10)] is direct-detected by using two 1GHz-bandwidth InGaAs PIN photodiodes operating at room temperature, one for each of the two polarization modes. The resulting photocurrents are amplified by a 40dB-gain amplifier, sampled by an analog-to-digital (A-D) board, and stored for analysis. The overall sensitivity of Bob's preamplified receiver is measured to be 660 photons/bit for 10^{-9} error probability.

As shown in Fig. 4(right), the 100km-long WDM line consists of two 40-channel 100GHz-spacing arrayed-waveguide gratings (AWGs), two 50km spools of single-mode fiber (Corning, SMF-28), and an in-line EDFA with an output isolator. Along with the quantum-noise protected 0.25Gbps encrypted-data channel, two 10Gbps channels of classical data traffic also propagate through the described WDM line. Light from two DFB lasers on the 100GHz ITU grid (1546.9nm and 1553.3nm) is mixed on a 3dB coupler, where one output is terminated and the other enters a 10GHz-bandwidth fiber-coupled Mach-Zender type LiNbO$_3$ intensity modulator (IM). The IM is driven by an amplified 10Gbps pseudo-random bit sequence (PRBS) generated by a pattern generator of $(2^{31}-1)$ period. The PRBS modulated-channels (hereafter referred to as PRBS channels) then pass through an EDFA to compensate for losses before entering, and being spectrally separated by AWG1. By introducing approximately one meter fiber length difference between the separated PRBS channels before combining them into the 100km-long WDM line with AWG2, the bit sequences of the two channels are shifted by 50 bits. This shift reduces temporal correlations between the two PRBS channels, thereby more effectively simulating random, real-world data traffic. The 100km-long WDM line is loss compensated by an in-line EDFA. The 10dB power loss in the

FIG. 4: Left, transmitter/receiver setup: G1, RF power amplifier; OA1, low-noise EDFA followed by a Bragg-grating filter; G2, RF signal amplifier. Right, WDM network setup: OA1, low-noise EDFA; G3, IM driver; OA2, in-line EDFA followed by an optical isolator; OA3, EDFA.

first 50km spool of fiber (0.2dB/km loss) is compensated by 10dB of saturated gain from the in-line EDFA. The overall loss of the line is therefore 15dB, where 10dB come from the second 50km spool of fiber and the remaining 5dB from the two AWGs (2.5dB each).

After propagating through the WDM line the channels are separated by AWG3. Either of the two PRBS channels is amplified with a 20dB gain EDFA (OA3) and the group-velocity-dispersion (GVD) is compensated by a -1530ps/nm dispersion-compensation module (DCM). While the GVD introduced in the WDM line is approximately 1700ps/nm, the DCM used is sufficient for our demonstration. The amplified, GVD-compensated PRBS channel is detected using an InGaAs PIN-TIA receiver (RCVR) and analyzed for errors by a 10Gbps bit-error-rate tester (BERT). Bit-error rates for each PRBS channel are measured separately using the BERT.

Figure 5(a)(left) shows the optical spectrum of the light after AWG2 measured with 0.01nm resolution bandwidth. The launch powers in the quantum channel and in each of the PRBS channels are -25dBm and 2dBm, respectively. An eye pattern of the 1546.9nm PRBS channel at launch is shown in Fig. 5(a)(right). Measuring after AWG2 (i.e., at launch), neither PRBS channel showed any error in 10 terabits of pseudo-random data communicated. Figure 5(b)(left) shows the optical spectrum (0.01nm resolution bandwidth) of the light received after the second 50km spool of fiber. This figure clearly shows the 10dB loss in signal power of all the channels and the accompanying 10dB increase in the amplified-spontaneous-emission dominated noise floor. An eye pattern of the 1546.9nm PRBS channel, post dispersion compensation, is shown in Fig. 5(b)(right). While the effect of the residual GVD is clearly visible in the eye pattern, the bit-error rate for each of the PRBS channels remains nearly "error free" at 5×10^{-11}. Neither the bit-error rates nor the eye patterns of the PRBS channels change

FIG. 5: (a): Optical spectrum (left) and eye pattern (right) of a PRBS channel at launch [after AWG2 in Fig. 4(right)]. (b): Optical spectrum (left) and eye pattern (right) of a PRBS channel at the end of the line [before AWG3 in Fig. 4(right)].

when the quantum channel is turned off.

Figure 6 shows results of 5000 A-D measurements (one of the two detector outputs) of a 9.1Mb bitmap file transmitted on the encrypted channel from Alice to Bob (top) and to Eve (bottom) through the 100km-long WDM line at 250Mbps data rate. The insets show the respective decoded images. In this experiment, actions of Eve are physically simulated by Bob starting with an incorrect secret-key. Clearly, a real eavesdropper would aim to make better measurements by placing herself close to Alice and implementing a more optimized quantum measurement. While Fig. 6 does not explicitly demonstrate Eve's inability to distinguish logical ones from zeros, it does, show that a simple bit decision is impossible. In the current setup, the 12-bit D-A conversion allows Alice to
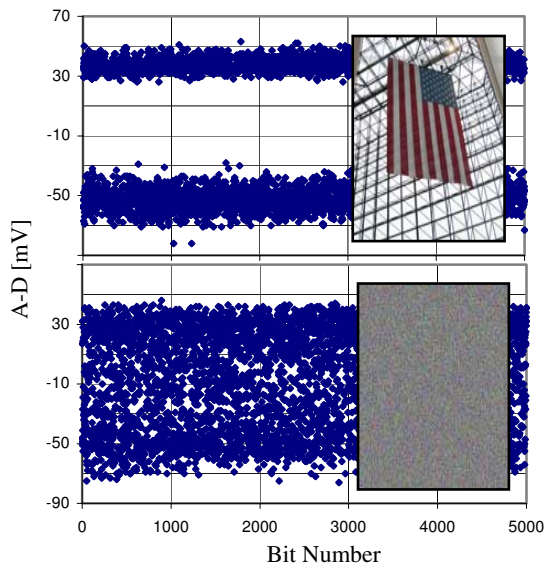
FIG. 6: 5-kbit segments of 9.1-Mbit transmissions through the WDM link. Insets, the received bit-map images. Top, Bob's detection; bottom, Eve's detection.

generate and transmit 4094 distinct polarization states ($M = 2047$ bases). The numerical calculation used to plot Fig. 3(right) then shows that for -25dBm launch power at 250Mbps (500Mbps line rate, $|\alpha|^2 \approx 20,000$) and $M = 2047$, Eve's maximum obtainable information in an individual attack on the message is less than 10^{-14} bits/bit.

B. Time-mode implementation

While technically possible, as demonstrated above, the polarization-state alignment required at the receiver by the polarization-mode scheme makes it much less attractive than a polarization-insensitive version with equivalent performance. The time-mode implementation is *totally* polarization-state insensitive and is therefore much more desirable for performing quantum-noise–protected data encryption over real-world WDM networks.

As with the polarization-mode implementation, a description of the time-mode experimental setup naturally breaks into two parts: the transmitter/receiver pair and the WDM fiber line. We first describe the transmitter/receiver pair. As illustrated in Fig. 7(left), -25dBm of power from a 1550.9nm-wavelength DFB laser is projected into Alice's 10GHz-bandwidth fiber-coupled PM. Driven by the amplified output of a 12-bit D-A board, the modulator introduces a relative phase (0 to 2π radians) between temporally neighboring symbols. A 4.4-kb software LFSR, which is implemented on a PC, yields a running-key that, when combined with the data bit, instructs the generation of one of the two states described in Eqs. (3) and (4) at a 650Mbps data rate. Before leaving the transmitter, the encrypted signal is amplified with an EDFA (OA1) to a saturated output power of 2dBm.

On passing through the 200km-long WDM line [shown in Fig. 7(right), *Crypto. in* and *Crypto. out*), the received light is amplified by another EDFA (OA2) with $\simeq 30$dB of small-signal gain and a noise figure very close to the quantum limit (NF $\simeq$ 3dB). The light then passes through a pair of 10GHz-bandwidth polarization-maintaining-fiber-coupled PMs oriented orthogonally with respect to each other so that the $\hat{x}$ ($\hat{y}$) polarization mode of the first modulator projects onto the $\hat{y}$ ($\hat{x}$) mode of the second modulator. The effect of such concatenation is to apply an optical phase modulation that is independent of the polarization state of the incoming light. The relative phase shift introduced by Bob's modulator pair is determined by the running-key R generated through a software LFSR in Bob's PC and applied via the amplified output of a second D-A board. After this phase shift has been applied, the relative phase between temporally neighboring states is 0 or π (differential phase-shift keying), differentially corresponding to a 0 or 1.

The decrypted signal then passes through a fiber-coupled optical circulator and into a temporally asymmetric Michelson interferometer with one bit-period round-trip path-length delay between the two arms. Use of Faraday mirrors (FM) in the Michelson interferometer ensures good polarization-state overlap at the output, yielding high visibility interference. The interferometer is path length stabilized with a PZT and dither-lock circuit.

Light from the two outputs of the interferometer is direct-detected by using two room temperature 1GHz-bandwidth InGaAs PIN photodiodes set up in a difference photocurrent configuration. The resulting photocurrent is either sampled by an A-D board and stored for analysis, or put onto a communications signal analyzer (CSA) to observe eye patterns.

As shown in Fig. 7(right), the 200km-long WDM line consists of two 100GHz-spacing AWGs, two 100km spools of single-mode fiber (Corning, SMF-28) and an in-line EDFA with an input isolator. Along with the quantum-noise protected 650Mbps encrypted-data channel, two 10Gbps channels of classical data traffic also propagate through the first 100km of the described WDM line. Light from two DFB lasers with wavelengths on the 100GHz ITU grid (1550.1nm and 1551.7nm) is mixed on a 3dB coupler, where one output is terminated and the other enters a 10GHz-bandwidth fiber-coupled Mach-Zender type LiNbO$_3$ intensity modulator (IM). The IM is driven by an amplified 10Gbps PRBS generated by a bit-error-rate tester (BERT) of $(2^{31}-1)$ period. The PRBS-modulated channels (hereafter referred to as PRBS channels) then pass through an EDFA to compensate for losses before entering and being spectrally separated by AWG1. Partial decorrelation of the PRBS channels is achieved by introducing approximately one meter fiber length difference ($\simeq$ 50 bits) between the channels before combining them into the WDM line with

FIG. 7: Left: Transmitter/receiver setup. G1, RF power amplifier; OA2, low-noise EDFA followed by a 25GHz-passband Bragg-grating filter; PMF, polarization-maintaining fiber; Circ., optical circulator. Right: 200km in-line amplified line. IM, 10Gbps intensity modulator; DCM, dispersion-compensation module; RCVR, 10Gbps InGaAs PIN-TIA optical receiver; G2, 10Gbps modulator driver

AWG2. On launch (i.e., after AWG2), the optical power is -2dBm/channel for all three channels.

After propagating through the first 100km of fiber (20dB of loss) and the in-line EDFA (23dB of gain), the channels are separated by AWG3 (3dB of loss). Either of the two PRBS channels is amplified with a 10dB gain EDFA and the GVD is partially compensated by a -1530ps/nm DCM. The amplified, GVD-compensated PRBS channel is detected using an InGaAs PIN-TIA receiver (RCVR) and analyzed for errors by the BERT. Note that the reason that the PRBS channels do not propagate through the entire 200km line is because our DCM only provides enough compensation for 100km of fiber. Figure 8(a)(left) shows the optical spectrum of the light measured after AWG2 with 0.01nm resolution bandwidth. The launch power in the quantum channel and in each of the PRBS channels is -1.5dBm. An eye pattern of the 1550.1nm PRBS channel at launch is shown in Fig. 8(a)(right). Measuring after AWG2 (i.e., at launch), neither PRBS channel showed any errors in 10 terabits of pseudo-random data communicated. Figure 8(b)(left) shows the optical spectrum (0.01nm resolution bandwidth) of the light received after the in-line amplifier (100km of fiber). An eye pattern of the 1550.1nm PRBS channel, post dispersion compensation, is shown in Fig. 8(b)(right). As in the polarization-mode implementation, the bit-error rate for each of the PRBS channels remained nearly "error free" at 5×10^{-11} despite the incomplete GVD compensation. Neither the bit-error rates nor the eye patterns of the PRBS channels changed when the quantum channel was turned off.

Figure 9 shows the eye patterns for encrypted 650Mbps $(2^{15} - 1)$-bit-PRBS and 1Mb-bitmap-file transmissions (insets) as measured by Bob (top) and Eve (bottom). In these experiments, Bob is located at the end of the 200km-long line and Eve is located at the transmitter (Alice). Eve's actions are physically simulated by using

FIG. 8: (a): Optical spectrum (left) and eye pattern of a PRBS channel (right) at launch [after AWG2 in Fig. 7(right)]. (b): Optical spectrum (left) and eye pattern of a PRBS channel (right) after in-line amplification [before AWG3 in Fig. 7(right)].

Bob's hardware, but starting with an incorrect secret-key. While Fig. 9(bottom) does not explicitly demonstrate Eve's inability to distinguish neighboring coherent states on the phase circle, it does, however, show that a simple bit decision is impossible. The Q-factor for Bob's eye pattern, as measured on the CSA, was 12.3.

In all of the time-mode implementation experiments, the coherent states are transmitted using non-return-to-zero (NRZ) format. The return-to-zero-like appearance of Bob's eye pattern is due to non-zero rise time of the optical phase modulation. This phenomena is also observed in traditional NRZ-DPSK systems. The apparent banding of Eve's measurements at the top and bottom of the eye pattern is due to the sinusoidal transfer function of the temporally asymmetric interferometer used for
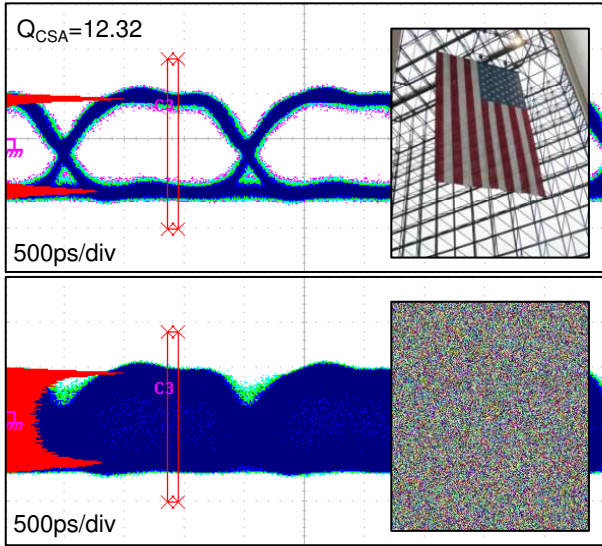
FIG. 9: Top: Eye pattern and histogram of Bob's decrypted signal after 200km propagation in the WDM line. Bottom: Eye pattern and histogram of Eve's measurements at the transmitter. Insets, received 1Mb bitmap file transmissions.

demodulation. Despite this apparent banding, the eavesdropper's probability of error is equal for every transmitted bit. If an eavesdropper were to, say, perform optical heterodyne detection, a uniform distribution of phases would be observed.

In the current setup, the 12-bit D-A conversion allows Alice to generate and transmit 4094 distinct phase states ($M = 2047$ bases). Although we simulate an eavesdropper by placing Bob's equipment at the transmitter, a real eavesdropper would aim to make the best measurements allowed by quantum mechanics (just as in the polarization-mode implementation). The numerical calculation used to plot Fig. 3(left) shows that for -25dBm signal power at 650Mbps ($\approx 40,000$ photons/bit) with $M = 2047$, Eve's maximum obtainable information in an individual attack on the message would be less than 10^{-15} bits/bit.

V.   DISCUSSION AND SUMMARY

In summary, we have developed schemes towards the cryptographic objective of practical data encryption by using the fundamental and irreducible quantum-measurement uncertainty of coherent states. Unlike currently deployed deterministic encrypters whose security relies solely on unproven computational complexity, we offer a new quantum-mechanical vehicle to quantifiable information-theoretic security through high-speed randomized encryption. Furthermore, we have clearly specified a set of security criteria for the cryptographic service of data encryption (which are different from those for key generation) and considered some optimal quantum attacks on our scheme. While we have yet to explicitly determine the level of information-theoretic security provided by our scheme under a general attack (which may correspond to finding λ_1, λ_2), our scheme does provide a physical layer of quantum-noise randomization that can only enhance the security of a message already encrypted with a traditional deterministic cipher.

Experimentally, we have implemented and demonstrated two high-speed versions of the $\alpha\eta$ data-encryption protocol using both polarization and time modes, and evaluated the schemes' performances through active WDM lines. Whereas the polarization-mode experiments have demonstrated the efficacy of the data-encryption protocol, the polarization independent time-mode experiments have demonstrated a technology that is "drop-in" compatible with the existing optical telecommunications infrastructure.

[1] G. Vernam, J. Am. I. Electrical En. **45**, 109 (1926).
[2] B. Schneier, *Applied Cryptography, 2nd Edition* (John Wiley and Sons, Inc., New York, 1996).
[3] J. Daemen and V. Rijmen, in *Smart Card Research and Applications, LNCS 1820*, edited by J. J. Quisquater and B. Schneier (Springer-Verlag, 2000), pp. 288–296.
[4] C. Bennett and G. Brassard, in *Proceedings of the IEEE International Conference on Computers, Systems, and Signal Processing, Bangalore, India* (1984), pp. 175–179.
[5] A. Ekert, Physics Review Letters **67**, 661 (1991).
[6] N. Gisin, G. Ribordy, W. Tittel, and H. Zbinden, Reviews of Modern Physics **74**, 145 (2002).
[7] W. Tittel, J. Brendel, H. Zbinden, and N. Gisin, Physics Review Letters **84**, 4737 (2000).
[8] T. Jennewein, C. Simon, G. Weihs, H. Weinfurter, and A. Zeilinger, Physics Review Letters **84**, 4729 (2000).
[9] H. Yuen, quant-ph/0311061 (2004).
[10] G. Barbosa, E. Corndorf, P. Kumar, and H. Yuen, Physics Review Letters **90**, 227901 (2003).
[11] E. Corndorf, G. Barbosa, C. Liang, H. Yuen, and P. Kumar, Optics Letters **28**, 2040 (2003).
[12] J. Massey, Proceedings of the IEEE **76**, 533 (1988).
[13] U. Maurer, Journal of Cryptology **5**, 53 (1992).
[14] R. Rivest and A. Sherman, in *Advances in Cryptology: Proceedings of Crypto 82*, edited by D. Chaum, R. Rivest, and A. Sherman (Plenum Press, New York, 1983), pp. 145–163.
[15] E. Corndorf, G. Kanter, C. Liang, and P. Kumar, in *2004*

Conference on Lasers Electro Optics (CLEO'04) post-deadline, San Francisco, CA (2004).

[16] E. Corndorf, G. Kanter, C. Liang, and P. Kumar, in *Quantum Information and Computation II*, edited by E. Donkor, A. R. Pirich, and H. E. Brandt (2004), vol. 5436, pp. 12–20.

[17] T. Cover and J. Thomas, *Elements of Information Theory* (John Wiley and Sons, Inc., New York, 1991).

[18] C. Shannon, Bell System Technical Journal **27**, 379 (1948).

[19] C. Shannon, Bell System Technical Journal **28**, 656 (1949).

[20] T. Nishioka, T. Hasegawa, H. Ishizuka, K. Imafuku, and H. Imai, Physics Letters A **327**, 28 (2004).

[21] H.P. Yuen,E. Corndorf P. Kumar and R. Nair, quant-ph/0407067, submitted to Phy. Lett. A (2004).

[22] G. Barbosa, Physics Review A **68**, 052307 (2003).

[23] Yuen's KCQ approach includes schemes for key generation that depend on the fact that $H(\mathbf{X}|\mathbf{Y_E}, \mathbf{K}) \neq 0$. In the regime in which $\alpha\eta$ operates, $H(\mathbf{X}|\mathbf{Y_E}, \mathbf{K})$ is effectively zero.